INTERNATIONAL JOURNAL FOR NUMERICAL METHODS IN ENGINEERING
Int. J. Numer. Meth. Engng 2006; **0**:0 *Prepared using* nmeauth.cls *[Version: 2002/09/18 v2.02]*

Green's Function Evaluation for Three Dimensional Exponentially Graded Elasticity

R. Criado[1], L. J. Gray[2], V. Mantič[1,*] and F. París[1]

[1] *Group of Elasticity and Strength of Materials, School of Engineering, University of Seville Camino de los Descubrimientos s/n, E-41092 Sevilla, Spain*
[2] *Computer Science and Mathematics Division, Oak Ridge National Laboratory Oak Ridge, TN 37831-6367, USA*

SUMMARY

The numerical implementation of the Green's function for an isotropic exponentially graded three dimensional elastic solid is reported. The formulas for the nonsingular 'grading term' in this Green's function, originally deduced by Martin et al., *Proc. R. Soc. Lond. A, 458, 1931-1947, 2000*, are quite complicated, and a small error in one of the formulas is corrected. The evaluation of the fundamental solution is tested by employing indirect boundary integral formulation using a Galerkin approximation to solve several problems having analytic solutions. The numerical results indicate that the Green's function formulas, and their evaluation, are correct. Copyright © 2006 John Wiley & Sons, Ltd.

KEY WORDS: Functionally graded materials, boundary integral equation, boundary element method, Galerkin approximation.

1. INTRODUCTION

Although a relatively new area of study, Functionally Graded Materials (FGMs) have many existing and potential applications [1, 2], including bio-medical [3, 4], construction [5], and geomechanics [6, 7]. This paper is concerned with the numerical solution of three dimensional elasticity problems in an FGM, based upon the commonly employed exponential grading model: the shear modulus is assumed to vary in a specified direction (say, z) as

$$\mu = \mu_0 e^{2\beta z}, \tag{1}$$

and the Poisson ratio $0 \leq \nu \leq 0.5$, μ_0 and the grading parameter β are assumed constant.

Previous elasticity computations in FGMs have employed the Finite Element Method (FEM). In particular, special graded elements have been developed by Kim and Paulino [8, 9],

*Correspondence to: Group of Elasticity and Strength of Materials, School of Engineering, University of Seville, Camino de los Descubrimientos s/n, E-41092 Sevilla, Spain
E-mail: mantic@esi.us.es

Received September 22, 2006

Naghabadi and Kordheili [10] and Santare *et al.* [11, 12] to more effectively deal with the material property variation.

Linear elastic analysis via boundary integral equations [13, 14, 15] can be advantageous, notably for problems wherein volume re-meshing becomes the principal difficulty with FEM – *e.g.*, crack propagation, flaw detection, contact, or shape optimization. Moreover, for an FGM in which μ varies rapidly over the volume, a highly refined FEM mesh would be required to obtain an accurate solution, and a boundary integral approach would again be attractive. However, a non-homogeneous medium presents a serious problem for a boundary integral formulation, as a Green's function (fundamental solution) is required to transform the partial differential equation. For the Laplace and Helmholtz equations, fundamental solutions have been developed for a general non-homogeneous medium [16, 17, 18, 19], and closed form, relatively simple, Green's functions exist for exponentially graded media [20, 21, 22]. See also [23] and references therein for work aimed at deriving Green's functions under more general conditions.

For an exponentially graded three dimensional isotropic material, the fundamental displacement tensor $\boldsymbol{\mathcal{U}}(P,Q)$ has recently been derived by Martin *et al.* [24] (the corresponding two dimensional result can be found in [25]). As yet there has been no numerical implementation of $\boldsymbol{\mathcal{U}}$, and the primary goal of this work is to begin this development of boundary integral algorithms for graded elasticity. The displacement tensor $\boldsymbol{\mathcal{U}}(P,Q)$ consists of an exponential prefactor multiplying two terms: the isotropic Kelvin solution, plus a grading contribution that is expressed in terms of several one- and two-dimensional integrals. The formulas for the grading term are quite complex, and indeed there is a small error in one expression in [24] that is corrected in this paper. It therefore seems best to thoroughly check the implementation of $\boldsymbol{\mathcal{U}}(P,Q)$, before moving on to consider its derivatives. This development and testing of the Green's function is accomplished herein.

The primary means of providing confidence in the correctness of the Green's function algorithm will be an indirect boundary integral formulation, wherein the displacements are expressed as the integral of the Green's function times a source density. A Boundary Element Method (BEM) procedure based on a Galerkin approximation of this equation will be employed to solve Dirichlet problems having known analytic solutions. Each of these topics, namely Green's function evaluation, the indirect boundary integral equation, exact FGM solutions and numerical results, will be discussed in detail below.

2. GRADED GREEN'S FUNCTION

In this section, the Green's function formulas obtained in [24] are summarized, as briefly as possible; further details can of course be found in this reference. In addition to defining the notation necessary for the discussion of the computational work, this will also permit correcting a small error in this derivation.

The equations of equilibrium in terms of stresses for an exponentially graded solid, neglecting body forces, are

$$\sigma_{ij,j} = 0, \tag{2}$$

where the linear elastic constitutive law is

$$\sigma_{ij}(\boldsymbol{x}) = c_{ijk\ell}(\boldsymbol{x})\epsilon_{k\ell}(\boldsymbol{x}), \tag{3}$$

$\epsilon_{k\ell}$ being the strains expressed through displacements as

$$\epsilon_{k\ell} = \frac{1}{2}\left(u_{k,\ell} + u_{\ell,k}\right), \tag{4}$$

and the elastic constants satisfying

$$c_{ijk\ell}(\boldsymbol{x}) = C_{ijk\ell}\, e^{2\boldsymbol{\beta}\cdot\boldsymbol{x}}. \tag{5}$$

Here $\boldsymbol{\beta}$ is the vector defining the direction of the grading, and $\beta = \|\boldsymbol{\beta}\|$ governs the exponential variation. Simplifying to an isotropic solid, the elastic constants can be expressed in terms of the Lamé parameters

$$C_{ijk\ell} = \lambda_0 \delta_{ij}\delta_{k\ell} + \mu_0\left(\delta_{ik}\delta_{j\ell} + \delta_{i\ell}\delta_{jk}\right), \tag{6}$$

and the exponential grading can be expressed in terms of Lamé constants as

$$\lambda = \lambda_0 e^{2\boldsymbol{\beta}\cdot\boldsymbol{x}}, \quad \mu = \mu_0 e^{2\boldsymbol{\beta}\cdot\boldsymbol{x}},$$

where $\lambda/\mu = \lambda_0/\mu_0 = 2\nu/(1-2\nu)$, ν the (constant) Poisson ratio. Notice, that Young elasticity modulus E is also exponentially graded:

$$E = E_0 e^{2\boldsymbol{\beta}\cdot\boldsymbol{x}}, \tag{7}$$

where $E_0 = \mu_0\left(3\lambda_0 + 2\mu_0\right)/\left(\lambda_0 + \mu_0\right)$.

As derived in [24], the expression of the fundamental solution $G_{j\ell}(Q,P)$, giving the fundamental displacement in the j-direction at the point Q due to a point load in the ℓ-direction at P, can be written in matrix form as:

$$\mathbf{G}(Q,P) = \exp\{-\boldsymbol{\beta}\cdot(Q+P)\}\,\left[\mathbf{G}^0(Q-P) + \mathbf{G}^g(Q-P)\right]. \tag{8}$$

The function $\mathbf{G}^0$ is the well known Kelvin solution for a homogeneous isotropic material (with elastic constants μ_0 and ν), and therefore available in closed form,

$$G^0_{j\ell}(Q-P) = \frac{1}{16\pi\mu_0(1-\nu)r}\,\left((3-4\nu)\,\delta_{j\ell} + r_{,j}\,r_{,\ell}\right). \tag{9}$$

Here $r = \|Q-P\|$ and $r_{,j}$ denotes the derivative of r with respect to the j^{th} coordinate of Q. The contribution $\mathbf{G}^g$ due to the material nonhomogeneity, to be called the grading term, can be written as

$$G^g_{j\ell}(Q-P) = -\frac{1}{4\pi\mu_0 r}\left(1-\mathrm{e}^{-\beta r}\right)\,\delta_{j\ell} + A_{j\ell}(Q-P), \tag{10}$$

where $A_{j\ell}$, as discussed below, has a fairly complicated expression in terms of one and two dimensional integrals. Note that the relatively simple diagonal contribution is continuous at $r=0$, and will not present any problem in the integrations. We further note that both $\mathbf{G}^0$ and $\mathbf{G}^g$ are functions of $\boldsymbol{r} = Q-P$, the Green's function departs from this property only through the exponential pre-factor in (8).

To give the specific form for $A_{j\ell}$, let us define an orthogonal system of coordinates $\{\boldsymbol{n},\boldsymbol{m},\hat{\boldsymbol{\beta}}\}$ where $\boldsymbol{n}$ and $\boldsymbol{m}$ are orthonormal vectors in the plane perpendicular to $\boldsymbol{\beta}$, $\hat{\boldsymbol{\beta}} = (\hat{\beta}_1,\hat{\beta}_2,\hat{\beta}_3) = \boldsymbol{\beta}/\beta$. For example, the components of $\{\boldsymbol{n},\boldsymbol{m}\}$ can be chosen as

$$\boldsymbol{n} = \beta_0^{-1}(\beta_3, 0, -\beta_1), \quad \boldsymbol{m} = (\beta\beta_0)^{-1}(-\beta_1\beta_2, \beta_0^2, -\beta_2\beta_3), \tag{11}$$

as long as $\beta_0 \equiv (\beta_1^2 + \beta_3^2)^{1/2} \neq 0$. For this system we have the corresponding spherical coordinates for $\boldsymbol{r} = Q - P$, (r, Θ, Φ), with $\hat{\boldsymbol{\beta}}$ as the polar axis,

$$\boldsymbol{r} \cdot \boldsymbol{n} = r \sin\Theta \cos\Phi, \quad \boldsymbol{r} \cdot \boldsymbol{m} = r \sin\Theta \sin\Phi, \quad \boldsymbol{r} \cdot \hat{\boldsymbol{\beta}} = r \cos\Theta, \tag{12}$$

where $0 \leq \Theta \leq \pi$ and $0 \leq \Phi \leq 2\pi$.

With these definitions, the (uncorrected) expression for $A_{j\ell} = A_{j\ell}(r, \Theta, \Phi)$ given in [24] is

$$\begin{aligned} A_{j\ell}(Q-P) = &- \alpha \frac{\pi}{2} \sum_{s=0}^{2} \sum_{n=0}^{2} \int_0^{\pi/2} \mathcal{R}_s^{(n)}(\Phi,\theta)\, \mathrm{e}^{-|k(\Theta,\theta)| y_s(\theta)}\, I_n(K(\Theta,\theta) y_s(\theta))\, \sin\theta \, \mathrm{d}\theta \\ &- \alpha \sum_{s=0}^{2} \int_{\theta_m(\Theta)}^{\pi/2} \mathcal{R}_s^{(0)}(\theta)\, \sin\theta \int_{\eta_m(\Theta,\theta)}^{\pi/2} \sinh\left(\Psi_s(\Theta,\theta,\eta)\right)\, \mathrm{d}\eta \, \mathrm{d}\theta \\ &+ \alpha \sum_{s=0}^{2} \int_{\theta_m(\Theta)}^{\pi/2} \mathcal{R}_s^{(2)}(\Phi,\theta)\, \sin\theta \int_{\eta_m(\Theta,\theta)}^{\pi/2} \sinh\left(\Psi_s(\Theta,\theta,\eta)\right)\, \cos 2\eta \, \mathrm{d}\eta \, \mathrm{d}\theta \\ &+ \alpha \sum_{s=1}^{2} \int_{\theta_m(\Theta)}^{\pi/2} \mathcal{R}_s^{(1)}(\Phi,\theta)\, \sin\theta \int_{\eta_m(\Theta,\theta)}^{\pi/2} \cosh\left(\Psi_s(\Theta,\theta,\eta)\right)\, \sin\eta \, \mathrm{d}\eta \, \mathrm{d}\theta, \end{aligned} \tag{13}$$

where

$$\alpha = \frac{\beta}{2\pi^2 \mu_0 (1-\nu)}, \tag{14}$$

and we now proceed to define the extensive notation introduced in this equation. First, $I_n(x)$ is the modified first kind Bessel function of order n, and the integration limits θ_m and η_m are defined by

$$\begin{aligned} \theta_m(\Theta) &= \left|\tfrac{1}{2}\pi - \Theta\right|, \\ |k(\Theta,\theta)| &= K(\Theta,\theta) \sin\eta_m(\Theta,\theta), \end{aligned} \tag{15}$$

where $k(\Theta,\theta) = \beta r \cos\theta \cos\Theta$ and $K(\Theta,\theta) = \beta r \sin\theta \sin\Theta$, and the range of θ guarantees that η_m is well defined (this function will be discussed further below). The argument of the hyperbolic functions is

$$\Psi_s(\Theta,\theta,\eta) = K(\Theta,\theta) y_s(\theta) \left(\sin\eta_m(\Theta,\theta) - \sin\eta\right), \tag{16}$$

where, defining

$$q(\theta) = 1 + \frac{2\nu}{1-\nu} \sin^2(\theta), \tag{17}$$

we have $q(\theta) \geq 1$ due to $0 \leq \nu \leq 0.5$, and the functions y_s are given by

$$y_0 = 1, \quad y_1 = \sqrt{q(\theta) + \sqrt{q^2(\theta) - 1}}, \quad y_2 = \sqrt{q(\theta) - \sqrt{q^2(\theta) - 1}}, \tag{18}$$

$\sqrt{\frac{1-\sqrt{\nu}}{1+\sqrt{\nu}}} \leq y_2 \leq 1 \leq y_1 \leq \sqrt{\frac{1+\sqrt{\nu}}{1-\sqrt{\nu}}}$. The functions $\mathcal{R}_s^{(n)}$ are

$$\begin{aligned} \mathcal{R}_s^{(0)}(\theta) &= \mathrm{i}\mathcal{M}_s^{(0)}(\theta), \quad s = 0,1,2, \\ \mathcal{R}_s^{(2)}(\Phi,\theta) &= -\mathrm{i}\mathcal{M}_s^{(2)}(\Phi,\theta), \quad s = 0,1,2, \\ \mathcal{R}_0^{(1)}(\Phi,\theta) &= 0, \\ \mathcal{R}_s^{(1)}(\Phi,\theta) &= -\left(\mathcal{M}_s^{(1)}(\Phi,\theta) + \widetilde{\mathcal{M}}_s^{(1)}(\Phi,\theta) \operatorname{sgn}(k(\Theta,\theta))\right), \quad s = 1,2, \end{aligned} \tag{19}$$

and $\mathcal{M}_s^{(n)}$, the result of integrations obtained via residue calculations, have the following definitions:

$$\begin{aligned}\mathcal{M}_0^{(n)}(\Phi,\theta) &= \frac{f_n(\mathrm{i})}{2\mathrm{i}\,D(\mathrm{i})},\\ \mathcal{M}_s^{(n)}(\Phi,\theta) &= \frac{f_n(\mathrm{i}y_s(\theta))}{(1-y_s(\theta)^2)\,D'(\mathrm{i}y_s(\theta))}, \quad s=1,2,\end{aligned} \tag{20}$$

for $n=0,2$, and

$$\mathcal{M}_s^{(1)}(\Phi,\theta) = \frac{f_1(\mathrm{i}y_s(\theta))}{D'(\mathrm{i}y_s(\theta))}, \quad \widetilde{\mathcal{M}}_s^{(1)}(\Phi,\theta) = \frac{\tilde{f}_1(\mathrm{i}y_s(\theta))}{D'(\mathrm{i}y_s(\theta))}, \quad s=1,2. \tag{21}$$

The last set of expressions needed to define $\mathcal{M}_s^{(n)}$ are

$$\begin{aligned}f_0(x) &= \tfrac{1}{2}\{8\nu x^4-(x^2+1)(2x^2q(\theta)+1)\}(n_jn_\ell+m_jm_\ell)\sin^2\theta\\ &\quad+\left\{8\nu x^4\sin^2\theta+(x^2+1)[x^2-(2x^2q(\theta)+1)\cos^2\theta]\right\}\hat{\beta}_j\hat{\beta}_\ell,\\ f_1(x) &= -x^3(4\nu-1)(s_j(\Phi)\hat{\beta}_\ell-\hat{\beta}_js_\ell(\Phi))\sin\theta,\\ \tilde{f}_1(x) &= -\tfrac{1}{2}\mathrm{i}(s_j(\Phi)\hat{\beta}_\ell+\hat{\beta}_js_\ell(\Phi))(2x^2q(\theta)+1)\sin 2\theta,\\ f_2(x) &= -\tfrac{1}{2}[8\nu x^4-(x^2+1)(2x^2q(\theta)+1)]\big\{n_j(n_\ell\cos 2\Phi+m_\ell\sin 2\Phi)\\ &\quad+m_j(n_\ell\sin 2\Phi-m_\ell\cos 2\Phi)\big\}\sin^2\theta,\\ s_j(\Phi) &= n_j\cos\Phi+m_j\sin\Phi,\\ D(x) &= x^4+2x^2q(\theta)+1, \quad D'(x)=4x^3+4xq(\theta).\end{aligned} \tag{22}$$

Given the lengthy derivation and the complexity of the resulting expression for $A_{j\ell}$, it is not entirely surprising that there might be an error. The existence of an error was indicated by computational results showing a discontinuity in $G_{j\ell}$ for $r\neq 0$, which cannot be correct. For a specific calculation, the discontinuity appeared in the $(1,3)$, $(3,1)$, $(2,3)$ and $(3,2)$ components of the Green function. As clearly visible in Figure 1, in which A_{23} is plotted as a function of Q_2 and Q_3 on the plane $Q_1=1.0$, the problem occurs between the regions $Q_3<0$ and $Q_3>0$, the source P being at the origin and the grading direction $\hat{\boldsymbol{\beta}}=(0,0,1)$.

The next section will therefore present the appropriate correction to the Green's function formulas.

3. CORRECTION TO $\widetilde{M}_{j\ell}^{(1)}$

The term that is responsible for the observed discontinuity in $G_{j\ell}^g(Q-P)$ comes from the last integral expression in (13) for $A_{j\ell}$ which takes the form:

$$-\alpha\sum_{s=1}^{2}\int_{\theta_m(\Theta)}^{\pi/2}\left(\mathcal{M}_s^{(1)}(\Phi,\theta)+\widetilde{\mathcal{M}}_s^{(1)}(\Phi,\theta)\mathrm{sgn}(k(\Theta,\theta))\right)\sin\theta\int_{\eta_m(\Theta,\theta)}^{\pi/2}\cosh\left(\Psi_s(\Theta,\theta,\eta)\right)\,\sin\eta\mathrm{d}\eta\,\mathrm{d}\theta. \tag{23}$$

Let us consider the following term (denoted as T_1) from this expression:

$$T_1=-\alpha\sum_{s=1}^{2}\int_{\theta_m(\Theta)}^{\pi/2}\widetilde{\mathcal{M}}_s^{(1)}(\Phi,\theta)\,\mathrm{sgn}(k(\Theta,\theta))\sin\theta\int_{\eta_m(\Theta,\theta)}^{\pi/2}\cosh\left(\Psi_s(\Theta,\theta,\eta)\right)\,\sin\eta\,\mathrm{d}\eta\,\mathrm{d}\theta. \tag{24}$$

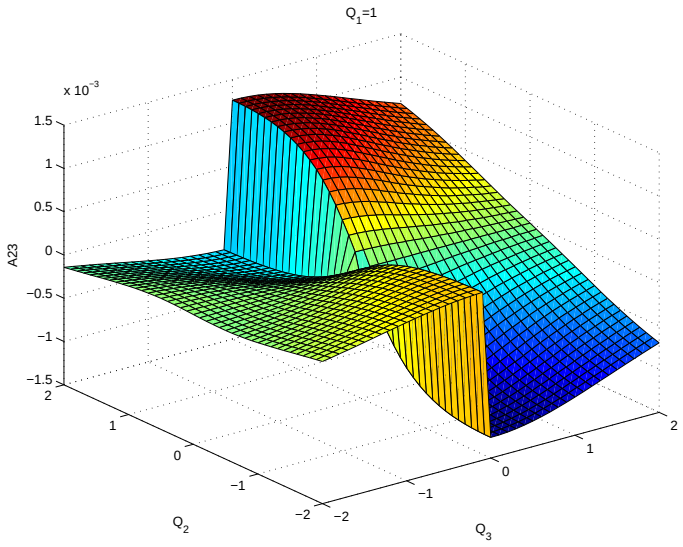

Figure 1. The function A_{23} based upon the original expressions for $P = (0, 0, 0)$ and $Q_1 = 1.0$, and the elasticity parameters $\mu_0 = 2.0$, $\nu = 0.35$ and $\boldsymbol{\beta} = (0, 0, 0.1)$.

T_1 comes from the term denoted as $\widetilde{M}^{(1)}_{j\ell}$ in [24] through the following relations:

$$A_{j\ell} = -\frac{\alpha}{2}\int_0^{\pi/2} M_{j\ell}(\theta)\,\sin\theta\,\mathrm{d}\theta, \quad \text{where} \quad M_{j\ell} = \sum_{n=0}^{2} M^{(n)}_{j\ell} + \widetilde{M}^{(1)}_{j\ell}. \tag{25}$$

$\widetilde{M}^{(1)}_{j\ell}$ has to be an odd function of k, and therefore vanishing where $\mathrm{sgn}(k(\Theta, \theta))$ changes sign. However, as will be discussed below, the formula given in [24] for $\widetilde{M}^{(1)}_{j\ell}$, used in the present work to obtain T_1, does not represent an odd function. Consequently, T_1 in the form (24) is not correct. These faults will be removed herein.

The initial integral expression for the quantity $\widetilde{M}^{(1)}_{j\ell}$, Eq. (5.5) in [24], was:

$$\widetilde{M}^{(1)}_{j\ell} = \int_{-\infty}^{\infty} \frac{\tilde{f}_1(x)}{D(x)}\,J_1(Kx)\,\mathrm{e}^{\mathrm{i}kx}\,\mathrm{d}x. \tag{26}$$

By noting that $\frac{\tilde{f}_1(x)}{D(x)}\,J_1(Kx)$, J_1 being the usual Bessel function, is an odd function of x, it is clear that $\widetilde{M}^{(1)}_{j\ell}$ is an odd function of k. However, according to [24], the expression for $\widetilde{M}^{(1)}_{j\ell}$ is supposed to be Eq. (5.13) with $\widetilde{\mathcal{M}}^{(1)}_s$ replacing $\mathcal{M}^{(1)}_s$, namely

$$\widetilde{M}^{(1)}_{j\ell} = 2\pi \sum_{s=1}^{2} \widetilde{\mathcal{M}}^{(1)}_s \Bigg\{ -\mathrm{e}^{-ky_s}\,I_1(Ky_s) + \frac{2}{\pi} H(K-k) \int_{\eta_0}^{\pi/2} \cosh\left(y_s[k - K\sin\eta]\right)\,\sin\eta\,\mathrm{d}\eta \Bigg\}, \tag{27}$$

where η_0 is defined via

$$k = K \sin \eta_0, \tag{28}$$

and $H(x)$ is the Heaviside function. Replacing the Bessel function $I_1(Ky_s)$ by its integral representation

$$2 \int_0^{\pi/2} \sinh (Ky_s \sin \eta) \, \sin \eta \, \mathrm{d}\eta = \pi I_1(Ky_s). \tag{29}$$

we obtain:

$$\widetilde{M}_{j\ell}^{(1)} = 4 \sum_{s=1}^{2} \widetilde{\mathcal{M}}_s^{(1)} \Big\{ -\mathrm{e}^{-ky_s} \int_0^{\pi/2} \sinh (Ky_s \sin \eta) \, \sin \eta \, \mathrm{d}\eta + H(K-k) \int_{\eta_0}^{\pi/2} \cosh \left(y_s[k - K \sin \eta]\right) \, \sin \eta \, \mathrm{d}\eta \Big\}. \tag{30}$$

It can be observed that when $k = 0$ (and thus $\eta_0 = 0$), $\widetilde{M}_{j\ell}^{(1)}$ is not necessarily zero, in contradiction to the fact that this function is odd with respect k.

It is however a simple matter to follow the procedures in [24] to correct the error in (30). Starting from (26) and replacing the Bessel function $J_1(Kx)$ with its integral formulation

$$J_1(Kx) = \frac{2}{\pi} \int_0^{\pi/2} \sin (Kx \sin \eta) \, \sin \eta \, \mathrm{d}\eta, \tag{31}$$

we first obtain

$$\widetilde{M}_{j\ell}^{(1)} = \frac{2}{\pi} \int_0^{\pi/2} \sin (Kx \sin \eta) \sin \eta \int_{-\infty}^{\infty} \frac{\tilde{f}_1(x)}{D(x)} \, \mathrm{e}^{\mathrm{i}kx} \, \mathrm{d}x \, \mathrm{d}\eta, \tag{32}$$

and subsequently using $\sin(z) = \frac{\mathrm{e}^{\mathrm{i}z} - \mathrm{e}^{-\mathrm{i}z}}{2\mathrm{i}}$, we obtain

$$\widetilde{M}_{j\ell}^{(1)} = \widetilde{M}_{+} + \widetilde{M}_{-}, \tag{33}$$

where

$$\widetilde{M}_{\pm} = \pm \frac{(-\mathrm{i})}{\pi} \int_0^{\pi/2} \sin \eta \int_{-\infty}^{\infty} \frac{\tilde{f}_1(x)}{D(x)} \, \mathrm{e}^{\mathrm{i}x(k \pm K \sin \eta)} \, \mathrm{d}x \, \mathrm{d}\eta. \tag{34}$$

These two integrals are evaluated by residues. For $\widetilde{M}_{+}$ the contour is taken in the upper halfplane, as $k + K \sin \eta > 0$, resulting in

$$\widetilde{M}_{+} = 2 \sum_{s=0}^{2} \widetilde{\mathcal{M}}_s^{(1)} \mathrm{e}^{-ky_s} \int_0^{\pi/2} \mathrm{e}^{-Ky_s \sin \eta} \, \sin \eta \, \mathrm{d}\eta. \tag{35}$$

For $\widetilde{M}_{-}$, however, $(k - K \sin \eta)$ can change sign if $k < K$, and thus there are two cases to consider. First, if $k > K$, the residue calculation can be carried out, as above in the upper half plane, resulting in

$$\widetilde{M}_{-} = -2 \sum_{s=0}^{2} \widetilde{\mathcal{M}}_s^{(1)} \mathrm{e}^{-ky_s} \int_0^{\pi/2} \mathrm{e}^{Ky_s \sin \eta} \, \sin \eta \, \mathrm{d}\eta. \tag{36}$$

For $0 \le k < K$ and η_0 defined in (28), $0 \le \eta_0 < \frac{1}{2}\pi$, the integral for $\widetilde{M}_-$ can be rewritten as

$$\begin{aligned}\widetilde{M}_- =& \frac{\mathrm{i}}{\pi}\int_0^{\eta_0} \sin\eta \int_{-\infty}^{\infty} \frac{\tilde{f}_1(x)}{D(x)}\,\mathrm{e}^{\mathrm{i}x(k-K\sin\eta)}\,\mathrm{d}x\,\mathrm{d}\eta \\ &+ \frac{\mathrm{i}}{\pi}\int_{\eta_0}^{\pi/2} \sin\eta \int_{-\infty}^{\infty} \frac{\tilde{f}_1(x)}{D(x)}\,\mathrm{e}^{-\mathrm{i}x(K\sin\eta-k)}\,\mathrm{d}x\,\mathrm{d}\eta. \end{aligned} \tag{37}$$

For $\eta < \eta_0$ the contour for the residue calculation lies in the upper halfplane, and in the lower halfplane when $\eta > \eta_0$. As $\frac{\tilde{f}_1(x)}{D'(x)}$ is an odd function of x, there is a change of sign in the lower halfplane, and the expression for $\widetilde{M}_-$ is

$$\begin{aligned}\widetilde{M}_- =& -2\sum_{s=1}^{2}\widetilde{\mathcal{M}}_s^{(1)}\left\{\mathrm{e}^{-ky_s}\int_0^{\eta_0}\mathrm{e}^{Ky_s\sin\eta}\,\sin\eta\,\mathrm{d}\eta + \mathrm{e}^{ky_s}\int_{\eta_0}^{\pi/2}\mathrm{e}^{-Ky_s\sin\eta}\,\sin\eta\,\mathrm{d}\eta\right\} \\ &\pm 2\sum_{s=1}^{2}\widetilde{\mathcal{M}}_s^{(1)}\left\{\mathrm{e}^{-ky_s}\int_{\eta_0}^{\pi/2}\mathrm{e}^{Ky_s\sin\eta}\,\sin\eta\,\mathrm{d}\eta\right\} \\ =& -2\sum_{s=1}^{2}\widetilde{\mathcal{M}}_s^{(1)}\left\{\mathrm{e}^{-ky_s}\int_0^{\pi/2}\mathrm{e}^{Ky_s\sin\eta}\,\sin\eta\,\mathrm{d}\eta - 2\int_{\eta_0}^{\pi/2}\sinh\left(y_s[k-K\sin\eta]\right)\sin\eta\,\mathrm{d}\eta\right\}. \end{aligned} \tag{38}$$

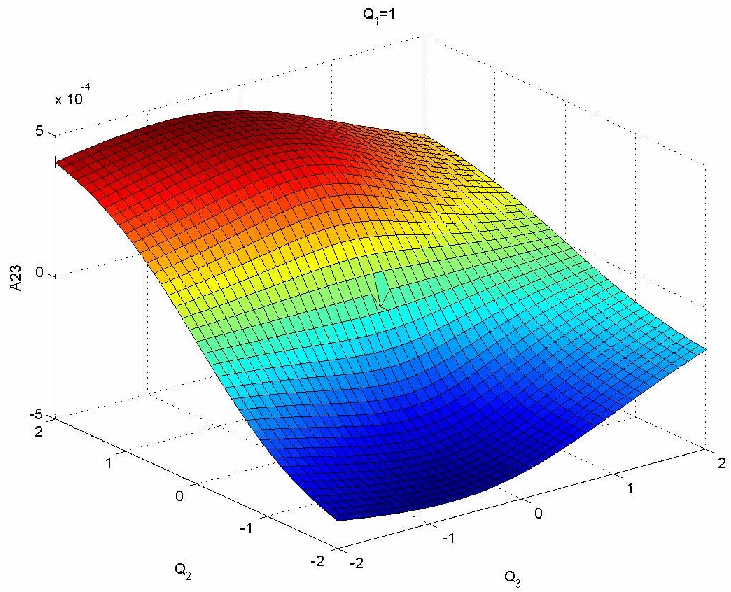

Figure 2. The function A_{23} based upon the new expressions for $P = (0, 0, 0)$ and $Q_1 = 1.0$, and the elasticity parameters $\mu_0 = 2.0$, $\nu = 0.35$ and $\boldsymbol{\beta} = (0, 0, 0.1)$.

The first integral is the same as that for $k > K$. Thus, for any non negative value of k and K

$$\widetilde{M}_{j\ell}^{(1)} = 2\pi\sum_{s=1}^{2}\widetilde{\mathcal{M}}_s^{(1)}\left\{-\mathrm{e}^{-ky_s}\,I_1(Ky_s) - \frac{2}{\pi}H(K-k)\int_{\eta_0}^{\pi/2}\sinh\left(y_s[k-K\sin\eta]\right)\sin\eta\,\mathrm{d}\eta\right\}, \tag{39}$$

which is Eq. (5.13) in [24], except that the cosh has been replaced by $-\sinh$. With this correction, $\widetilde{M}^{(1)}_{j\ell}$ is now an odd function with respect to k, and that changes the formula for T_1 into:

$$T_1 = \alpha \sum_{s=1}^{2} \int_{\theta_m(\Theta)}^{\pi/2} \widetilde{\mathcal{M}}^{(1)}_s(\Phi,\theta)\,\mathrm{sgn}(k(\Theta,\theta))\sin\theta \int_{\eta_m(\Theta,\theta)}^{\pi/2} \sinh\left(\Psi_s(\Theta,\theta,\eta)\right)\,\sin\eta\,\mathrm{d}\eta\,\mathrm{d}\theta. \quad (40)$$

To conclude this section, a plot of the same calculation of A_{23} as shown in Figure 1 now obtained using (40) is presented in Figure 2.

The expression for the grading term in the Green's function are clearly quite complicated, and, as just demonstrated, errors are possible. Numerical implementation and testing is therefore essential to establish confidence in the correctness of these formulas, and the remainder of the paper is focused on this goal.

4. COMPUTATIONAL FORM FOR $G_{j\ell}$

The purpose of this section is to give some further details on how the Green's function is computed. First, the Bessel functions in (13) are computed from their integral expressions,

$$I_1(Ky_s) = \frac{2}{\pi}\int_0^{\pi/2} \sinh\left(Ky_s\sin\eta\right)\,\sin\eta\,\mathrm{d}\eta, \quad (41)$$

$$I_n(Ky_s) = \frac{2}{\pi \mathrm{i}^n}\int_0^{\pi/2} \cosh\left(Ky_s\sin\eta\right)\,\cos n\eta\,\mathrm{d}\eta, \quad n = 0, 2. \quad (42)$$

Second, in addition to the correction of $\widetilde{M}^{(1)}_{j\ell}$, it is desirable to alter the formulas for $G_{j\ell}$ so as to avoid computing with the imaginary unit i. By noting that the polynomials $D(x)$ and $D'(x)$ are only evaluated for purely imaginary quantities, it is possible to change their definitions to

$$\begin{aligned} D(x) &= x^4 - 2x^2q + 1, \\ D'(x) &= -4x^3 + 4xq, \end{aligned} \quad (43)$$

keeping in mind that we keep the same notation but that now $D'(x)$ is not the derivative of $D(x)$. The corresponding changes in the functions f_i are

$$\begin{aligned} f_0(x) &= \tfrac{1}{2}\{8\nu x^4 - (-x^2+1)(-2x^2q+1)\}(n_jn_\ell + m_jm_\ell)\sin^2\theta \\ &\quad + \left\{8\nu x^4\sin^2\theta + (-x^2+1)[-x^2 - (-2x^2q+1)\cos^2\theta]\right\}\hat{\beta}_j\hat{\beta}_\ell, \\ f_1(x) &= x^3(4\nu-1)(s_j\hat{\beta}_\ell - \hat{\beta}_j s_\ell)\sin\theta, \\ \tilde{f}_1(x) &= -\tfrac{1}{2}(s_j\hat{\beta}_\ell + \hat{\beta}_j s_\ell)(-2x^2q+1)\sin 2\theta, \\ f_2(x) &= -\tfrac{1}{2}[8\nu x^4 - (-x^2+1)(-2x^2q+1)]\left\{n_j(n_\ell\cos 2\Phi + m_\ell\sin 2\Phi)\right. \\ &\quad \left. + m_j(n_\ell\sin 2\Phi - m_\ell\cos 2\Phi)\right\}\sin^2\theta, \end{aligned} \quad (44)$$

whereas $\mathcal{M}_s^{(n)}$ and $\mathcal{R}_s^{(n)}$ become

$$\begin{aligned}
\mathcal{M}_0^{(n)} &= \frac{f_n(1)}{2\,D(1)}, \quad n = 0, 2, \\
\mathcal{M}_s^{(n)} &= \frac{f_n(y_s)}{(1-y_s^2)\,D'(y_s)}, \quad n = 0, 2 \text{ and } s = 1, 2, \\
\mathcal{M}_s^{(1)} &= \frac{f_1(y_s)}{D'(y_s)}, \quad s = 1, 2, \\
\widetilde{\mathcal{M}}_s^{(1)} &= \frac{\tilde{f}_1(y_s)}{D'(y_s)}, \quad s = 1, 2,
\end{aligned} \tag{45}$$

$$\begin{aligned}
\mathcal{R}_s^{(0)} &= \mathcal{M}_s^{(0)}, \quad s = 0, 1, 2, \\
\mathcal{R}_s^{(2)} &= -\mathcal{M}_s^{(2)}, \quad s = 0, 1, 2, \\
\mathcal{R}_0^{(1)} &= 0, \\
\mathcal{R}_s^{(1)} &= -\left(\mathcal{M}_s^{(1)} + \widetilde{\mathcal{M}}_s^{(1)}\,\mathrm{sgn}(k(\Theta,\theta))\right), \quad s = 1, 2.
\end{aligned} \tag{46}$$

To summarize, the complete expression of $\mathbf{G}$ is:

$$\mathbf{G}(Q,P) = \exp\{-\boldsymbol{\beta}\cdot(Q+P)\}\,\left\{\mathbf{G}^0(Q-P) + \mathbf{G}^g(Q-P)\right\}, \tag{47}$$

where $\mathbf{G}^0$ is the Kelvin solution (9) and the grading term $\mathbf{G}^g$ is computed using

$$G^g_{j\ell}(Q-P) = -(4\pi\mu_0 r)^{-1}\left(1-\mathrm{e}^{-\beta r}\right)\,\delta_{j\ell} + A_{j\ell}(Q-P). \tag{48}$$

The numerically evaluated term $A_{j\ell}$ is composed of 5 integrals:

$$A_{j\ell} = -\frac{\beta}{4\pi\mu_0(1-\nu)}\,\mathcal{I}_1 - \frac{\beta}{2\pi^2\mu_0(1-\nu)}\,(\mathcal{I}_2 - \mathcal{I}_3 + \mathcal{I}_4 - \mathcal{I}_5) \tag{49}$$

where

$$\begin{aligned}
\mathcal{I}_1 &= \sum_{s=0}^{2}\sum_{n=0}^{2}\int_0^{\pi/2} \mathcal{R}_s^{(n)}(\theta)\,\mathrm{e}^{-|k|y_s}\,I_n(Ky_s)\,\sin\theta\,\mathrm{d}\theta, \\
\mathcal{I}_2 &= \sum_{s=0}^{2}\int_{\theta_m}^{\pi/2} \mathcal{R}_s^{(0)}\,\sin\theta\int_{\eta_m}^{\pi/2}\sinh\Psi_s\,\mathrm{d}\eta\,\mathrm{d}\theta, \\
\mathcal{I}_3 &= \sum_{s=0}^{2}\int_{\theta_m}^{\pi/2} \mathcal{R}_s^{(2)}\,\sin\theta\int_{\eta_m}^{\pi/2}\sinh\Psi_s\,\cos 2\eta\,\mathrm{d}\eta\,\mathrm{d}\theta, \\
\mathcal{I}_4 &= \sum_{s=1}^{2}\int_{\theta_m}^{\pi/2} \mathcal{M}_s^{(1)}\,\sin\theta\int_{\eta_m}^{\pi/2}\cosh\Psi_s\,\sin\eta\,\mathrm{d}\eta\,\mathrm{d}\theta, \\
\mathcal{I}_5 &= \sum_{s=1}^{2}\int_{\theta_m}^{\pi/2} \tilde{\mathcal{M}}_s^{(1)}\,\mathrm{sgn}(k)\,\sin\theta\int_{\eta_m}^{\pi/2}\sinh\Psi_s\,\sin\eta\,\mathrm{d}\eta\,\mathrm{d}\theta.
\end{aligned} \tag{50}$$

4.1. The function $\eta_m(\Theta, \theta)$

The lower limit function $\eta_m(\Theta, \theta)$ presents some complications for the numerical implementation, and thus this function is discussed in detail below. The arguments take values in the range $\Theta \in [0, \pi]$ and $\theta \in [\theta_m, \pi/2]$ (θ_m defined in (13)), and $\eta_m(\Theta, \theta)$ is defined via

$$|\beta r \cos\Theta \cos\theta| = \beta r \sin\Theta \sin\theta \, \sin\eta_m. \tag{51}$$

However, as $\beta \geq 0$, $r \geq 0$, $\sin\Theta \geq 0$ for $\Theta \in [0, \pi]$, and $\cos\theta \geq 0$, $\sin\theta \geq 0$ for $\theta \in [\theta_m, \pi/2]$, it follows that

$$\eta_m = \sin^{-1}\left[\mathrm{sgn}(\pi/2 - \Theta)\cot\theta\cot\Theta\right]. \tag{52}$$

This function is plotted in Figure 3 for $\Theta \in [0, \pi]$ and $\theta \in [\theta_m, \pi/2]$.

Note that $\eta_m(\Theta, \pi/2) = 0$, $\eta_m(\Theta, \theta_m) = \pi/2$, θ_m being defined in $(15)_1$, and that the derivative with respect to θ at this latter point is infinite. This can be seen in Figure 4, where $\eta_m(\Theta = \pi/2 - 0.0001, \theta)$ is plotted as a function of θ. Thus in the integrations, some care should be taken due to the rapid variation of η_m. Fortunately, for $\eta_m = \pi/2$ the η integral vanishes.

When $\Theta = \pi/2$, $\theta_m = 0$, and $\eta_m(\pi/2, \theta) \equiv 0$ except for the indeterminate point $\theta = 0$. By continuity, this value should be set to zero. Also, η_m is likewise undefined for $\Theta = 0$ or $\Theta = \pi$; however in this case $\theta_m = \pi/2$ and the θ interval is zero. However, in the numerical implementation these extreme points must be avoided.

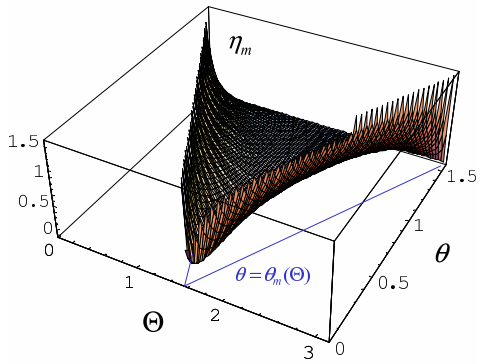

Figure 3. The function $\eta_m(\Theta,\ \theta)$, $\Theta \in [0, \pi]$ and $\theta \in [\theta_m, \pi/2]$.

5. GREEN'S FUNCTION PROPERTIES

It is important to note that the grading term $\mathbf{G}^g$ is bounded at $r = 0$. Thus, the graded Green's function $\mathbf{G}$ and the Kelvin solution $\mathbf{G}^0$ share the same singularity at $r = 0$. Otherwise, however, the behavior of $\mathbf{G}$ can be quite different from $\mathbf{G}^0$. In particular, even for a small value of β, the presence of the exponential coefficient in (8) means that significant differences appear in the farfield, $Q \to \pm\infty\hat{\boldsymbol{\beta}}$. Note that Lamé constants λ and μ go to zero in one direction and to infinity in the other, and thus the grading term must behave very differently than the Kelvin

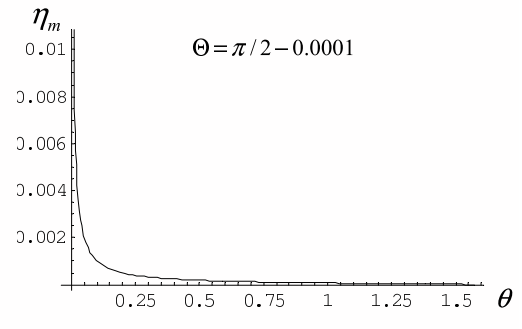

Figure 4. The function $\eta_m(\Theta = \pi/2 - 0.0001,\ \theta)$.

solution. As the grading term formulas are quite complex and provide little insight, this section will illustrate the properties of $\mathbf{G}$, mainly through graphs of function values.

5.1. Symmetry

For any Q and P, a fundamental solution for any elastic material must fulfill the reciprocity relation (as a consequence of Betti's theorem of reciprocity of work [26]):

$$G_{j\ell}(Q,P) = G_{\ell j}(P,Q). \tag{53}$$

For a homogeneous material the Green's function is also symmetric (observe that the source and field points are not interchanged):

$$G^0_{j\ell}(Q-P) = G^0_{\ell j}(Q-P), \tag{54}$$

and thus it is worth noting that this is not the case when the material is graded.

5.2. Discontinuity at $r = 0$

As noted above, the required divergent behavior of $\mathbf{G}$ at $r = 0$ is contained entirely in the Kelvin solution. Nevertheless, the behavior of the grading term at $r = 0$ is not simple. To illustrate this, assume that the grading is in the z-direction, $\boldsymbol{\beta} = (0,0,\beta)$, $\boldsymbol{n} = (1,0,0)$ and $\boldsymbol{m} = (0,1,0)$. Take the source point at the origin, $P = (0,0,0)$, and consider the grading term component G^g_{13} in the plane $Q_3 = 0$. For the Kelvin solution, (9), we have

$$G^0_{13} = \frac{1}{16\mu\, r\, \pi(1-\nu)}\, r_{,1}\, r_{,3}, \tag{55}$$

and as $r_{,3} = 0$ for $Q_3 = P_3 = 0$, $G^0_{13} = 0$.

For the grading term however, $G^g_{13} \neq 0$, and we now proceed to derive the expression for this component. Note that with $Q_3 = 0$, $0 = \boldsymbol{r}\cdot\hat{\boldsymbol{\beta}} = r\cos\Theta$, and thus $k(\Theta,\theta) = \beta r\cos\theta\,\cos\Theta = 0$ and $\eta_m = 0$. Moreover, $\beta_1 = 0$ forces $f_0(x) = 0$ and as only $n_1 = m_2 = 1$ are nonzero, also $f_2(x) = 0$; the nonzero contributions are therefore from $\widetilde{\mathcal{M}}^{(1)}_s$ and $\mathcal{M}^{(1)}_s$.

Simplifying even further, consider the value of A_{13} for $r \to 0$, in which case $K \to 0$. Then, A_{13} for small r is approximately

$$A_{13} \approx -\cos\Phi\, \frac{\beta(4\nu-1)}{2\pi^2\mu_0(1-\nu)} \sum_{s=1}^{2} \int_0^{\pi/2} \frac{y_s^3\,\sin^2\theta}{D'(y_s)}\,\mathrm{d}\theta. \tag{56}$$

As the coefficient, call it c, of $\cos\Phi$ is in general nonzero, A_{13} is discontinuous at $r = 0$, taking on all values in the interval $[-c, c]$ arbitrarily close to the source point P.

5.3. Plots in the neighbourhood of $r = 0$

Some of the above discussed properties of the graded Green's function will be illustrated in this section by its plots in the neighbourhood of the singular point, here defined at the origin of coordinates, $P = (0, 0, 0)$, in two planes, one perpendicular and the other parallel to the grading direction, here defined by $\boldsymbol{\beta} = (0, 0, \beta)$. In order to facilitate the understanding of the following plots, the point load direction, the displacement direction and the grading direction, respectively, are indicated by marks "F", "D" and "Bet", if possible.

The elastic material properties considered are $\mu_0 = 1$, $\nu = 0.3$, which implies $\lambda_0 = 1.5$, and $\beta = 0.1$

Consider first the plane $Q_3 = 0$ perpendicular to the grading direction. Thus, the elastic properties are constant in this plane.

The dominant character of the unbounded homogeneous term $\mathbf{G}^0$ over the bounded graded term $\mathbf{G}^g$ is clearly seen in Figures 5 - 8, where plotted components G_{11}, G_{22}, G_{33}, G_{12} and G_{21} show a form similar to the Kelvin fundamental solution. As follows from the considerations of the symmetries given by the point load direction, plane position and grading direction, it can be expected that: *i)* G_{11} and G_{22} have the same values changing Q_1 by Q_2, *i.e.* $G_{11}(Q_1, Q_2, 0) = G_{22}(Q_2, Q_1, 0)$, *ii)* $G_{12}(Q_1, Q_2, 0) = G_{21}(Q_1, Q_2, 0)$, and *iii)* G_{33} has the rotational symmetry in this plane. These facts have been confirmed by the plotted values of the Green's function.

According to the previous analysis, G_{13} is bounded, and similarly also G_{31}, G_{23} and G_{32} are bounded in the plane $Q_3 = 0$, because the corresponding homogeneous terms vanish there. Nevertheless, as also follows from this analysis these components of the Green's function are discontinuous (more precisely undetermined) at P. The form of this discontinuity is shown in Figures 9 - 12. Additionally, observing these plots, these components of the Green's function verify the following relations: $G_{13}(Q_1, Q_2, 0) = G_{31}(-Q_1, -Q_2, 0)$, $G_{23}(Q_1, Q_2, 0) = G_{32}(-Q_1, -Q_2, 0)$, $G_{13}(Q_1, Q_2, 0) = G_{23}(Q_2, Q_1, 0)$ and $G_{31}(Q_1, Q_2, 0) = G_{32}(Q_2, Q_1, 0)$, which can be easily deduced taking into account the point load direction, plane position, grading direction, and reciprocity relation (53).

Consider now the plane $Q_1 = 0$ parallel to the grading direction. Thus, the Lamé constants vary as functions of Q_3 in this plane.

The dominant character of $\mathbf{G}^0$ over $\mathbf{G}^g$ is seen in all Figures 13 - 16, where plotted components G_{11}, G_{22}, G_{33} and G_{23} again show a form similar to the Kelvin fundamental solution. Although, $G_{23}(0, Q_2, Q_3)$ is in general different from $G_{32}(0, Q_2, Q_3)$, due to the dominance of the homogenous term, the plots of both components show a form very similar to the Kelvin fundamental solution, where these components coincide as follows from its symmetry property. Thus, only G_{23} is plotted in Figure 16, for the sake of brevity.

Due to the fact that the plane $Q_1 = 0$ is the symmetry plane in the elastic problems given by the point force acting in the Q_2- or Q_3-directions, $G_{12}(0, Q_2, Q_3) = G_{13}(0, Q_2, Q_3) = 0$. Using reciprocity relation (53) it holds $G_{21}(0, Q_2, Q_3) = G_{12}(0, -Q_2, -Q_3) = 0$, and similarly for G_{31} and G_{13}. Thus, all these components of Green's function vanish in this plane.

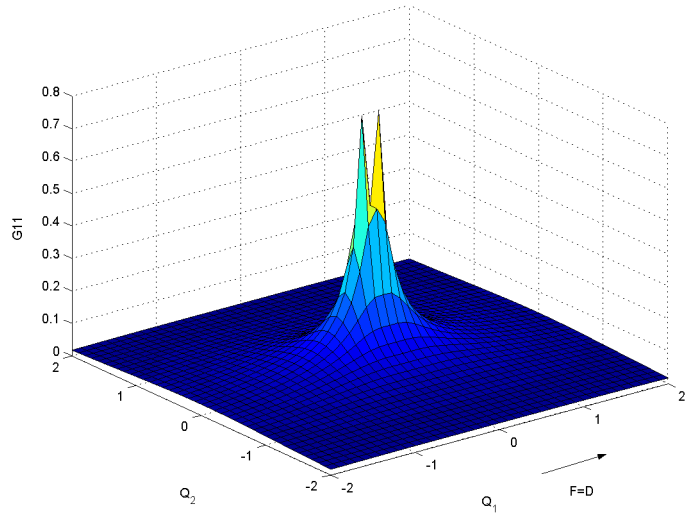

Figure 5. G_{11} in plane $Q_3 = 0$.

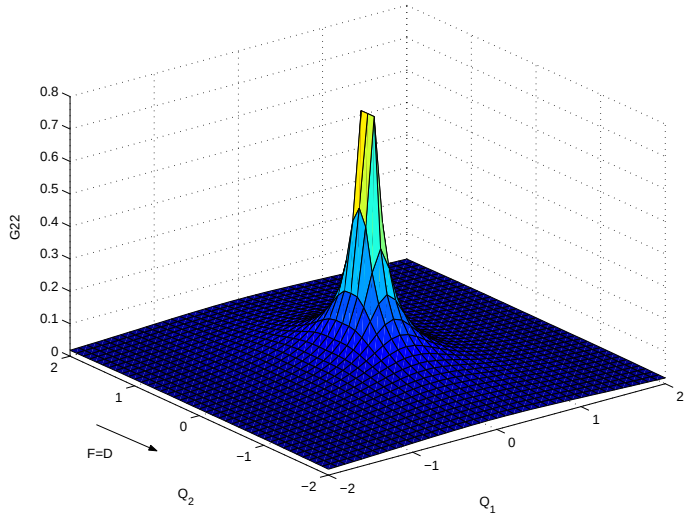

Figure 6. G_{22} in plane $Q_3 = 0$

6. INDIRECT BOUNDARY INTEGRAL FORMULATION

The confirmation that the formulas for the Green's function, and their numerical implementation, are correct can be accomplished with an 'indirect' boundary integral equation

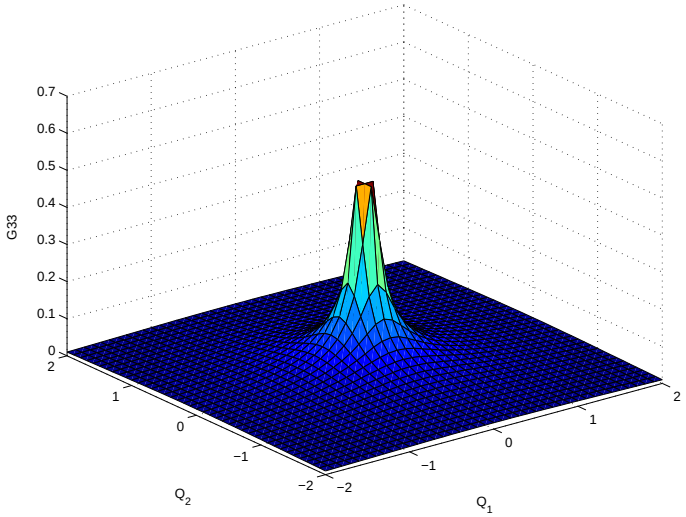

Figure 7. G_{33} in plane $Q_3 = 0$

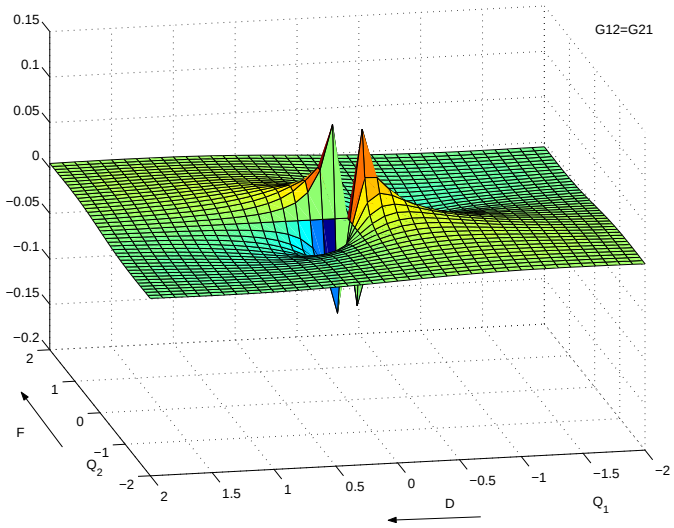

Figure 8. $G_{12} = G_{21}$ in plane $Q_3 = 0$

employing only the Green's function. The standard notation in the Boundary Element Method for the fundamental displacement tensor is $\boldsymbol{\mathcal{U}}(P, Q)$, and thus at the risk of some confusion, we switch to this notation. Recall, that in the notation of [24], the ℓ^{th} column of the Green's function contains the displacement solution due to a point load in the ℓ-direction. Thus, the

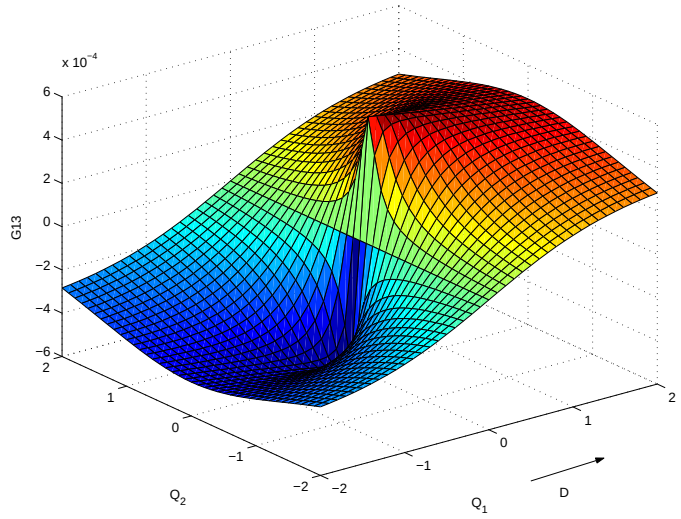

Figure 9. G_{13} in plane $Q_3 = 0$

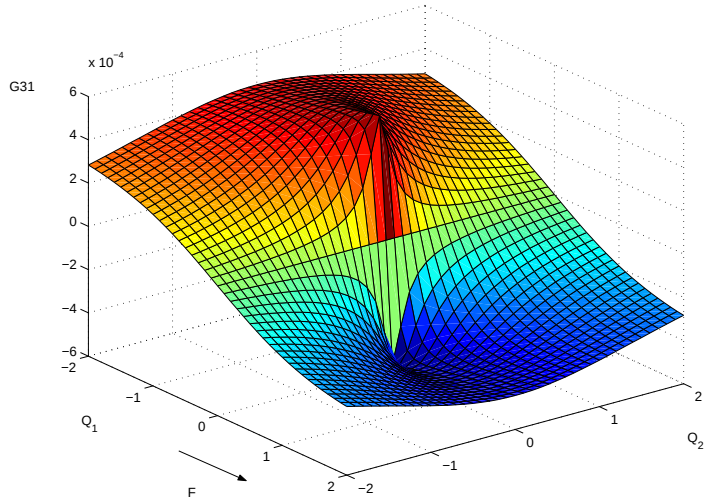

Figure 10. G_{31} in plane $Q_3 = 0$

indirect boundary integral equation for displacements on the solid boundary Σ writes as

$$\mathbf{u}(Q) = \int_{\Sigma} \boldsymbol{\mathcal{U}}(Q,P)\boldsymbol{\phi}(P)\,\mathrm{d}P, \tag{57}$$

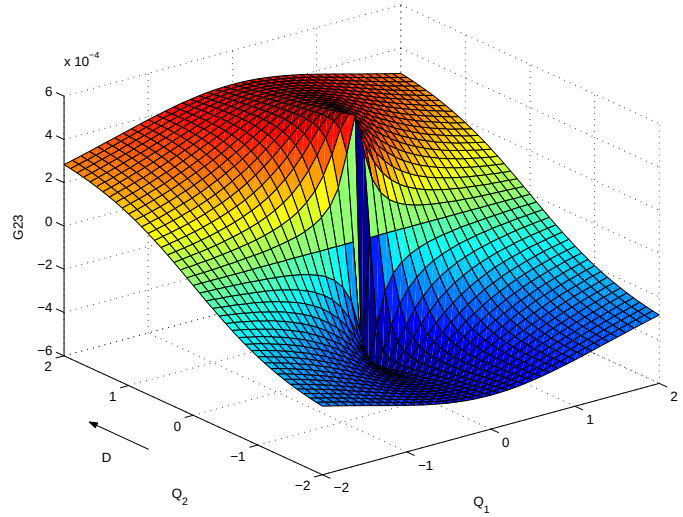

Figure 11. G_{23} in plane $Q_3 = 0$

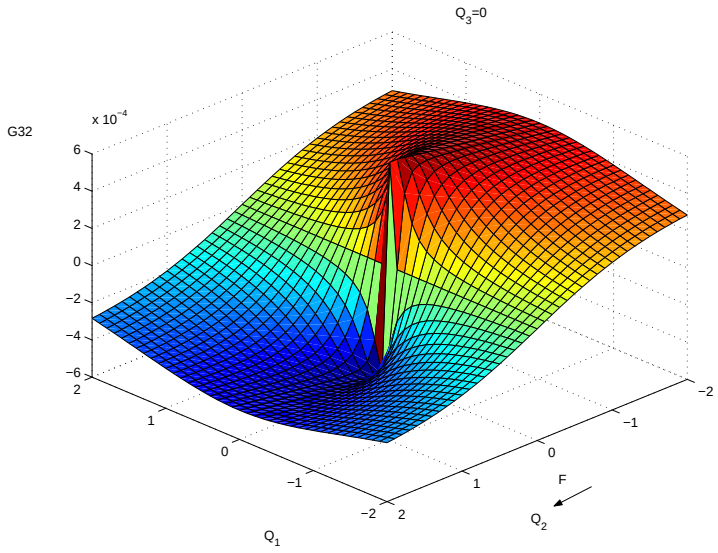

Figure 12. G_{32} in plane $Q_3 = 0$

where it is set $\boldsymbol{\mathcal{U}}(Q,P) = \mathbf{G}(Q,P)$. As discussed above, unlike for homogeneous materials, $\mathcal{U}_{j\ell}(Q,P) \neq \mathcal{U}_{\ell j}(Q,P)$ in general.

In (57), the displacement $\mathbf{u}(Q)$ is assumed to be a linear combination of the Green's function, the coefficient $\boldsymbol{\phi}(P)$ being an unknown source density on the boundary Σ. In a standard

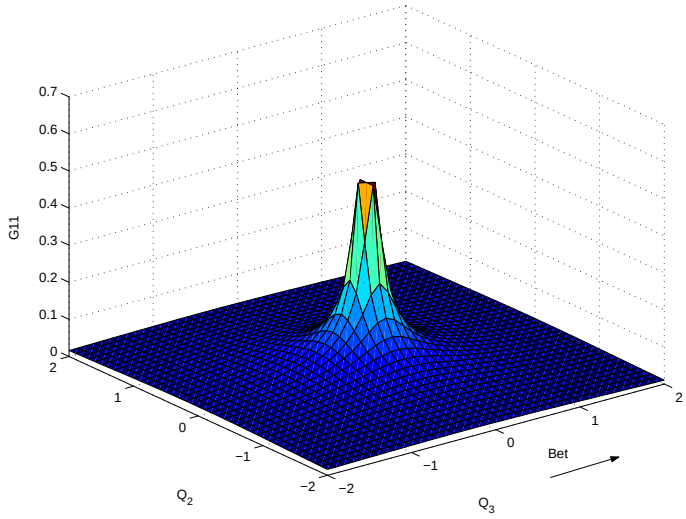

Figure 13. G_{11} in plane $Q_1 = 0$

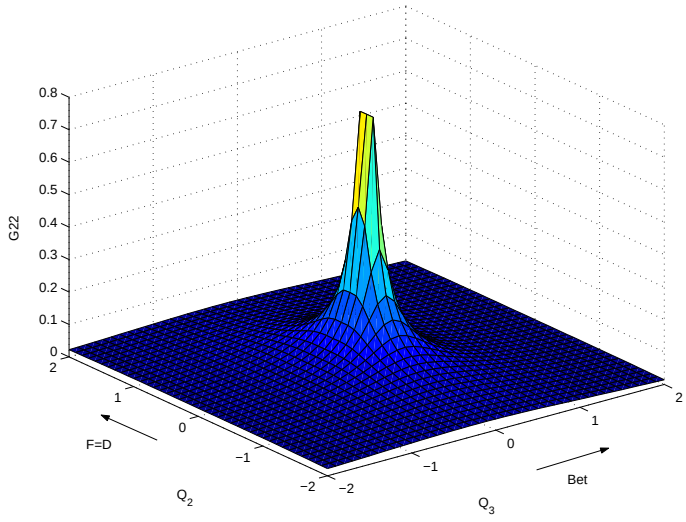

Figure 14. G_{22} in plane $Q_1 = 0$

(direct) boundary integral treatment, the function that multiplies $\boldsymbol{\mathcal{U}}^T$ is a physical quantity, the traction. This is not the case here, there is no direct physical relevance of $\boldsymbol{\phi}(P)$. In general, there are significant drawbacks to use an indirect first kind equation such as (57) [27], though indirect second kind equations are somewhat more successful [28]. An effective boundary

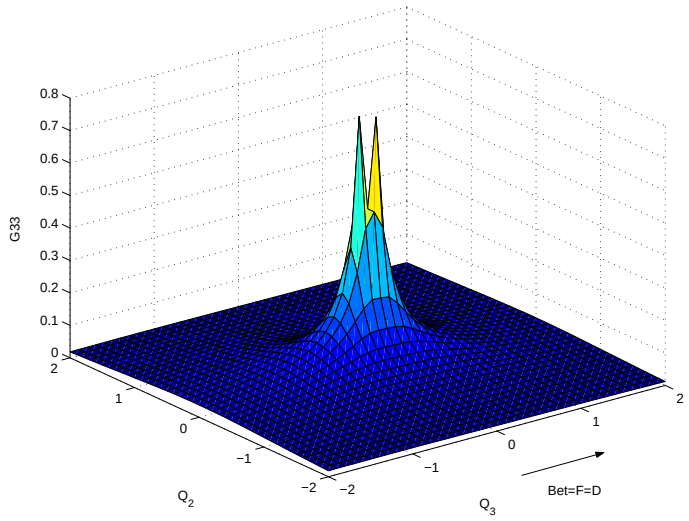

Figure 15. G_{33} in plane $Q_1 = 0$

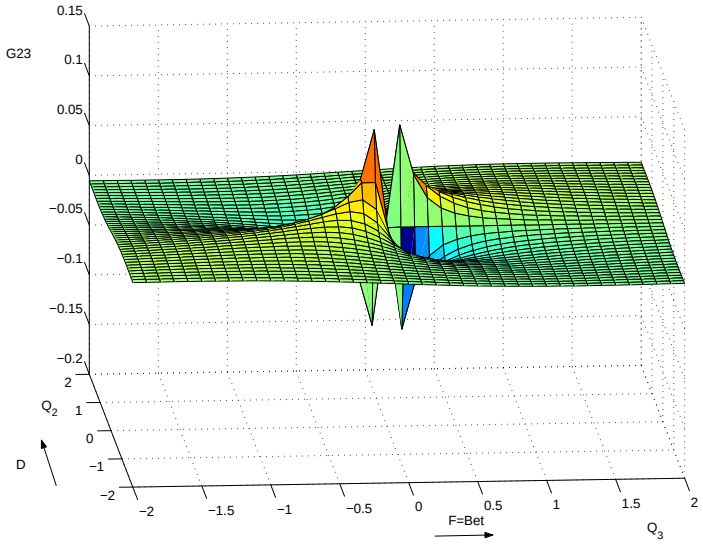

Figure 16. G_{23} in plane $Q_1 = 0$

integral equation treatment for graded materials will therefore require, at the very least, the ability to work with the traction kernel $\boldsymbol{\mathcal{T}}(P, Q)$ involving derivatives of the Green's function $\boldsymbol{\mathcal{U}}(P, Q)$. However, together with exact solutions of the FGM equations obtained in Section 7,

the indirect formulation will suffice for our purposes here, testing the evaluation of the Green's function $\boldsymbol{\mathcal{U}}(P,Q)$. The numerical results will be presented in Section 8.

A Galerkin approximation [14] of (57) will be employed to obtain the source density $\boldsymbol{\phi}(P)$. The equation to be solved numerically is therefore

$$\int_\Sigma \Psi_k(Q)\mathbf{u}(Q)\,\mathrm{d}Q = \int_\Sigma \Psi_k(Q) \int_\Sigma \boldsymbol{\mathcal{U}}(Q,P)\boldsymbol{\phi}(P)\,\mathrm{d}P\,\mathrm{d}Q, \tag{58}$$

where the Galerkin weight functions $\Psi_k(Q)$ are composed of the shape function employed to interpolate the boundary and the boundary functions $\mathbf{u}(Q)$ and $\boldsymbol{\phi}(P)$. For these approximations we choose to work with a 3-noded triangular element, defined using an equilateral triangle parameter space $\{\eta,\xi\}$, $-1 \le \eta \le 1$, $0 \le \xi \le \sqrt{3}(1-|\eta|)$, Figure 17. The three linear shape functions $\Psi_j(\eta,\xi)$ are given by

$$\Psi_1(\eta,\xi) = \frac{\sqrt{3}(1-\eta)-\xi}{2\sqrt{3}}, \quad \Psi_2(\eta,\xi) = \frac{\sqrt{3}(1+\eta)-\xi}{2\sqrt{3}}, \quad \Psi_3(\eta,\xi) = \frac{\xi}{\sqrt{3}}. \tag{59}$$

The parametric variables for the outer Q integration will be denoted by (η,ξ), and those for P by (η^*,ξ^*). Thus, for an element defined by nodal points $\{P_j = (x_j,y_j,z_j)\}$, the mapping from parameter space to the approximate boundary surface is

$$P(\eta^*,\xi^*) = \sum_{j=1}^{3}(x_j,y_j,z_j)\Psi_j(\eta^*,\xi^*). \tag{60}$$

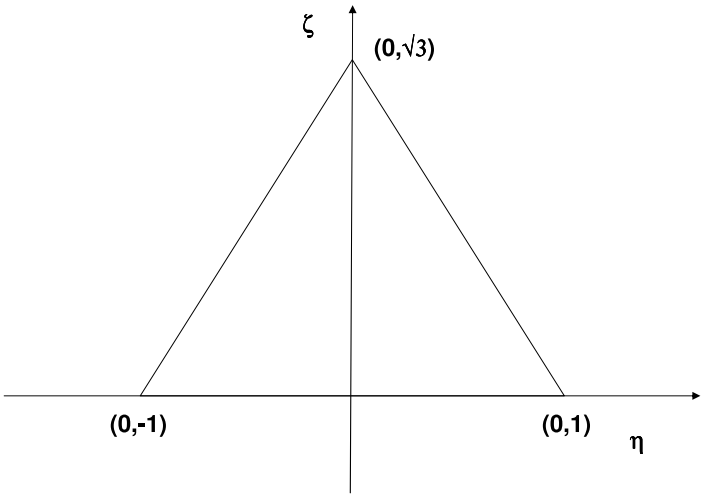

Figure 17. The equilateral triangle parameter space chosen to implement the linear interpolation.

The numerical implementation of (58) is relatively easy, in that the kernel function $\boldsymbol{\mathcal{U}}$ is only weakly singular, and moreover this singularity is only present in the analytic Kelvin solution term. The grading term itself is simply discontinuous at $Q = P$, see Section 5.2, and does not present a problem. Nevertheless, the methods discussed below for integrating $\boldsymbol{\mathcal{U}}$ will also apply directly to the $\boldsymbol{\mathcal{T}}$ kernel involving first order derivatives of $\boldsymbol{\mathcal{U}}$.

The hybrid analytical/numerical algorithms to be employed for Galerkin singular integration have been extensively discussed in [29, 30]; thus, the discussion will be limited to the adjustments needed to handle the graded Green's function. These modifications are primarily for handling the exponential factor in (8), and as these are essentially the same as the procedures employed for FGM thermal analysis [31], the discussion is kept to a minimum.

The singular integration techniques in [29] are based upon employing polar coordinate $\{\rho, \vartheta\}$ transformations centered at the singular point, and then integrating analytically (the rational functions of) ρ. Although the analytic integration for (58) is limited to the Kelvin solution part of $\boldsymbol{\mathcal{U}}$, it is nevertheless useful to also employ the polar coordinate transformation in the numerical integration of the grading term: the jacobian ρ will eliminate the discontinuity in this function at the singular point. For the analytic integration, the exponential prefactor in (8) is a minor complication. As discussed in [31], the exponential is easily handled via a Taylor series in ρ. Thus, for the coincident integral over an element E,

$$\int_E \Psi_k(Q) \int_E \boldsymbol{\mathcal{U}}(Q,P)\boldsymbol{\phi}(P)\,\mathrm{d}P\,\mathrm{d}Q, \tag{61}$$

the integrand is split as

$$\begin{aligned} \boldsymbol{\mathcal{U}} &= \mathrm{e}^{-\beta\,(Q_3+P_3)}\left[\boldsymbol{\mathcal{U}}^0 + \boldsymbol{\mathcal{U}}^g\right] \\ &= \left\{\left(\mathrm{e}^{-\beta\,(Q_3+P_3)} - \mathrm{e}^{-2\beta Q_3}\right)\boldsymbol{\mathcal{U}}^0 + \mathrm{e}^{-\beta\,(Q_3+P_3)}\,\boldsymbol{\mathcal{U}}^g\right\} + \mathrm{e}^{-2\beta Q_3}\,\boldsymbol{\mathcal{U}}^0. \end{aligned}$$

The two terms inside the braces can be integrated numerically, while the last term can be integrated analytically with respect to ρ, Q_3 being independent of ρ. (If desired, the second analytic integration detailed in [29] can also be carried out, again by employing a Taylor expansion of Q_3, which is no longer constant).

The adjacent edge and vertex singular integrations handled in the same manner: a Taylor expansion is employed to split off a part of the Kelvin term, this is integrated partially analytically, and the remainder treated numerically.

7. EXACT FGM SOLUTIONS

This section presents a set of analytic solutions for exponentially graded isotropic elastic solids, whose governing equations are given by (2-6), that can be employed to test the implementation of $\boldsymbol{\mathcal{U}}(Q,P)$. This set is based on the so-called *plane stress* solutions studied for three-dimensional homogeneous isotropic elastic solids, for instance, in [32, 33].

In addition to these analytic solutions, we also have the option to solve problems specified by an exterior concentrated load point. By fixing the source P_0 exterior to the chosen domain $\mathcal{D}$, the function $\boldsymbol{\mathcal{U}}(Q,P_0)$ 'should be' a solution inside $\mathcal{D}$. In this case, as discussed further below, both the boundary conditions and the 'exact' solution are computed from $\boldsymbol{\mathcal{U}}(Q,P_0)$.

7.1. Plane stress solutions

Let us consider an exponential grading in the z-direction. Let plane stress solutions be characterized (in a generalized sense) by $\sigma_{i3}(\boldsymbol{x}) = \sigma_{3i}(\boldsymbol{x}) = 0$ $(i = 1, 2, 3)$.

Let $\sigma^0_{ij}(\boldsymbol{x})$, $\epsilon^0_{ij}(\boldsymbol{x})$ and $u^0_i(\boldsymbol{x})$ $(i,j=1,2,3)$ with $\sigma^0_{i3}=\sigma^0_{3i}=0$ represent a classical plane stress solution in a homogeneous isotropic elastic solid with elastic properties E_0 and ν. Hence,

$$\begin{aligned}\epsilon^0_{ij} &= \frac{1+\nu}{E_0}\sigma^0_{ij} - \frac{\nu}{E_0}\sigma^0_{kk}\delta_{ij},\\ \epsilon^0_{ij} &= \frac{1}{2}\left(u^0_{i,j}+u^0_{j,i}\right).\end{aligned} \tag{62}$$

A general form and properties of such solutions can be find in [32, 33].

It is an easy matter to check that stresses, strains and displacements defined using the following *ansatz*:

$$\begin{aligned}\sigma_{ij}(\boldsymbol{x}) &= e^{2\beta z}\sigma^0_{ij}(\boldsymbol{x}),\\ \epsilon_{ij}(\boldsymbol{x}) &= \epsilon^0_{ij}(\boldsymbol{x}),\\ u_i(\boldsymbol{x}) &= u^0_i(\boldsymbol{x})\end{aligned} \tag{63}$$

represent an elastic solution in an exponentially graded isotropic solid verifying Eqs. (2-6). Hence, many analytic solutions of different complexity for three-dimensional graded solids, which can be used in different numerical tests, can be generated be means of (63). Notice, that the opposite statement holds as well, thus, any plane stress solution in an exponentially graded solid can be written using representation (63).

It should also be pointed out that (63), replacing $e^{2\beta z}$ by a $f(z)$, can also be applied to generate plane stress solutions in other functionally graded materials defined by any positive grading function $f(z)$, continuous or discontinuous.

7.1.1. Linear displacements It is interesting to observe that a general linear displacement field:

$$\mathbf{u} = \begin{pmatrix} a_1+b_1x+c_1y+d_1z\\ a_2+b_2x+c_2y+d_2z\\ a_3+b_3x+c_3y+d_3z\end{pmatrix} \tag{64}$$

representing rigid body translations and rotations and constant strain solutions has to verify

$$\begin{aligned}\beta\left(d_1+b_3\right)&=0,\\ \beta\left(d_2+c_3\right)&=0,\\ \beta\left(2\mu_0 d_3+\lambda_0\left(b_1+c_2+d_3\right)\right)&=0,\end{aligned} \tag{65}$$

which means that for $\beta\neq 0$ it corresponds to a plane stress solution discussed above.

7.1.2. Quadratic displacements Let us consider the classical three-dimensional solution for bending of an elastic isotropic homogeneous beam by a pair of moments about the y axis applied at its ends (the x-axis coinciding with the central line of the beam, the y- and z-axes being the principal axes of inertia of the cross section), see [34]. By substituting this solution into (63) the following solution with quadratic displacements in an exponentially graded material is obtained: $\sigma_{ij}=0$ except $\sigma_{11}=E_0e^{2\beta z}z=E(z)z$, and

$$\mathbf{u} = \begin{pmatrix} xz\\ -\nu yz\\ -\frac{1}{2}\left(x^2+\nu\left\{z^2-y^2\right\}\right)\end{pmatrix}. \tag{66}$$

7.2. Exterior Point Source

In addition to the above simple analytic solutions, a good 'self-consistency' check of $\boldsymbol{\mathcal{U}}(Q,P)$ can be carried out by using an exterior point source. If the point P_0 is exterior to the chosen domain $\mathcal{D}$, then the columns of $\boldsymbol{\mathcal{U}}(Q,P_0)$ 'should be' a valid displacement solution inside $\mathcal{D}$. We can therefore take this displacement $u_i(Q) = \mathcal{U}_{ik}(Q,P_0)$ as boundary conditions and solve for the $\boldsymbol{\phi}(P)$. With this density, interior values of displacement can be computed from

$$u_i(Q_I) = \int_\Sigma \mathcal{U}_{ik}(Q_I,P)\phi_k(P)\,\mathrm{d}P, \tag{67}$$

and compared to the expected value, namely $\mathcal{U}_{ik}(Q_I,P_0)$. Strictly speaking this is not an analytic solution, in that both the boundary conditions and the 'exact' solution are computed from the function being tested, $\boldsymbol{\mathcal{U}}(Q,P)$. The agreement of interior displacements would only confirm that $\boldsymbol{\mathcal{U}}$ is reproduced by its boundary values. Nevertheless, these tests may in fact be the most convincing. By putting the point load reasonably close to the boundary, and selecting a large value for the grading parameter β, the displacement boundary values and the source density will not be simple functions, and they will be strongly dependent upon the grading term in the fundamental solution expression (8).

8. NUMERICAL RESULTS

The problems discussed in the previous section will be solved numerically using the indirect integral equation (58). The chosen geometry, a graded sphere of radius 1 centered at the origin, is, for the most part, a matter of convenience. We are however restricted to domains with a smooth boundary surface Σ, as corners and edges in general present significant difficulties for the indirect approach [27].

In all of the tests, the elastic parameters were chosen as $\mu_0 = 1/2$ and $\nu = 1/3$. Hence, $\lambda_0 = 1$ and $E_0 = 4/3$. For small values of the grading parameter β the Kelvin solution will be the dominant contribution to $\boldsymbol{\mathcal{U}}$, and thus to test the evaluation of the grading term, $\beta \geq 0.1$. Thus, the variation in shear modulus over the volume of the sphere will be about 50% or more, and the grading term will contribute significantly.

The test procedure is as follows: the known exact solutions will provide displacement boundary conditions for (58), permitting the solution of the surface density $\boldsymbol{\phi}(P)$. The exact displacements at points Q_I interior to the sphere can then be compared with those computed using $\boldsymbol{\phi}(P)$ and (57), providing a test that $\boldsymbol{\mathcal{U}}$ satisfies the graded elasticity equations (2-6). For the exterior point load examples, however, the interior displacement is known only by evaluating $\boldsymbol{\mathcal{U}}(Q_I,P_0)$, and thus this is only a self-consistency check. However, as noted above, agreement in these examples would be strong evidence of the correctness of the implementation.

The first simple numerical test considers the following linear displacement field $\mathbf{u} = (x, 0, -\nu' z)$, with $\nu' = \frac{\nu}{1-\nu}$, as a particular case of (64-65), representing in fact a plane strain solution with respect to the y-direction. The corresponding stress field is $\sigma_{11} = E_0' e^{2\beta z}$ and $\sigma_{22} = \nu E_0' e^{2\beta z}$, with $E_0' = E_0/(1-\nu^2)$ and $\beta = 0.1$, and the remaining stress components vanish. Using the above solution as displacement boundary conditions on the unit sphere (discretized with 512 elements), the corresponding surface density was computed. With this solution, interior displacement values can then be computed, and the exact and computed

values along the x- and z-axes are presented in Tables I and II, exhibiting excellent agreement. Recall that the exact solution in displacements is independent of β, and the calculation has successfully "washed-out" the contributions of β to the Green's function.

Table I. The values of the displacement component u_x at interior points $(x, 0, 0)$ for the linear displacement solution.

Point	Exact	Computed
(0.0, 0.0, 0.0)	0.0	0.000000013
(0.1, 0.0, 0.0)	0.1	0.099873647
(0.2, 0.0, 0.0)	0.2	0.199750287
(0.3, 0.0, 0.0)	0.3	0.299634085
(0.4, 0.0, 0.0)	0.4	0.399531052
(0.5, 0.0, 0.0)	0.5	0.499449047
(0.6, 0.0, 0.0)	0.6	0.599398488
(0.7, 0.0, 0.0)	0.7	0.699402010
(0.8, 0.0, 0.0)	0.8	0.799502375
(0.9, 0.0, 0.0)	0.9	0.899365376

Table II. The values of the displacement component u_z at interior points $(0, 0, z)$ for the linear displacement solution.

Point	Exact	Computed
(0.0, 0.0, 0.0)	0.0	0.000149778
(0.0, 0.0, 0.1)	-0.05	-0.049809248
(0.0, 0.0, 0.2)	-0.1	-0.099769404
(0.0, 0.0, 0.3)	-0.15	-0.149733148
(0.0, 0.0, 0.4)	-0.2	-0.199703921
(0.0, 0.0, 0.5)	-0.25	-0.249684715
(0.0, 0.0, 0.6)	-0.3	-0.299676489
(0.0, 0.0, 0.7)	-0.35	-0.349682090
(0.0, 0.0, 0.8)	-0.4	-0.399714849
(0.0, 0.0, 0.9)	-0.45	-0.449736673

For the problem with quadratic displacements (66), the grading parameter was $\beta = 0.1$, and the sphere was discretized with 512 elements again. Figure 18 displays the computed and exact interior displacements along the line $x = y = z$, the results agreeing very well with the exact solution.

For the first exterior point load problem, the load point was $(0, \sqrt{2}, \sqrt{2})$, the force in the x-direction, $\beta = 0.1$, and the sphere was discretrized with 896 elements. The interior displacements u_y and u_z along the line $y = z = 0$, $0 < x < 1$ are shown in Figure 19. As discussed above, the values computed from (57) are compared with the displacements

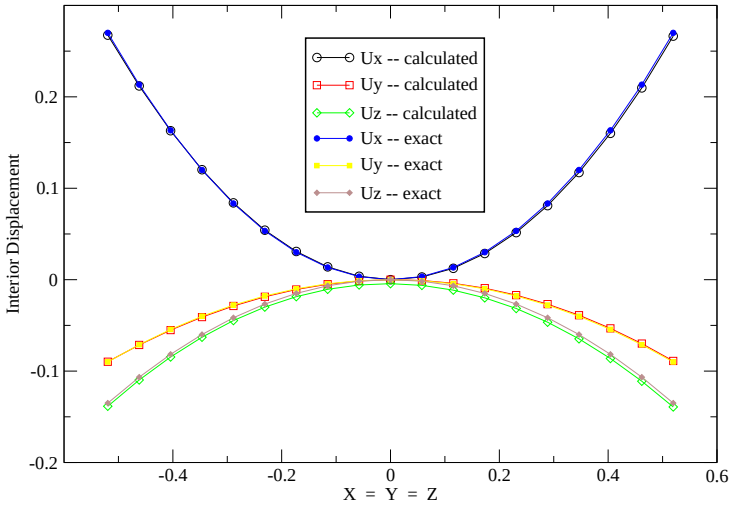

Figure 18. Interior displacement values at points (x, x, x) for $\beta = 0.1$ and quadratic displacements.

computed directly from the Green's function. The displacements u_x are almost constant, and thus the corresponding values are listed in Table III.

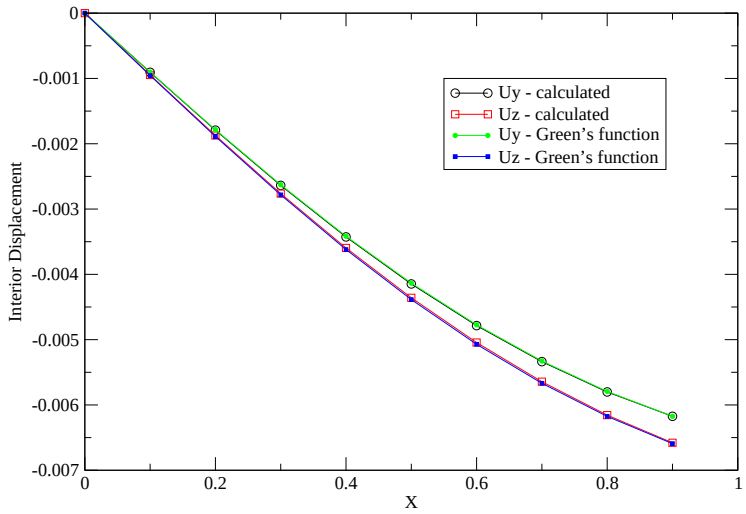

Figure 19. Interior displacement values at points $(x, 0, 0)$ for $\beta = 0.1$ and point load boundary conditions.

To make the point load test more challenging, the source was moved closer to the sphere, at $(0,\ 2\sqrt{2}/3,\ 2\sqrt{2}/3)$, the load direction was changed to the grading direction z, and the strength of the grading was increased to $\beta = 0.2$. For these calculations, the sphere was again discretized with 896 elements. The interior displacements u_y and u_z were computed along the lines $x = z = 0$, $0 < y < 1$, Figure 20, and $x = 0$, $y = z$, Figure 21. The u_x component is along

Table III. The values for the displacement component u_x for a point load located at $(0, \sqrt{2}, \sqrt{2})$, load in the x-direction, $\beta = 0.1$. The first column is computed directly from $\boldsymbol{\mathcal{U}}$, the second from (57) after solving (58).

Point	Green's Function	Computed
(0.0, 0.0, 0.0)	0.034140174	0.034019747
(0.1, 0.0, 0.0)	0.034151290	0.034032359
(0.2, 0.0, 0.0)	0.034182977	0.034068511
(0.3, 0.0, 0.0)	0.034230434	0.034123339
(0.4, 0.0, 0.0)	0.034286259	0.034189314
(0.5, 0.0, 0.0)	0.034341229	0.034256997
(0.6, 0.0, 0.0)	0.034385224	0.034315891
(0.7, 0.0, 0.0)	0.034408145	0.034355350
(0.8, 0.0, 0.0)	0.034400717	0.034365329
(0.9, 0.0, 0.0)	0.034355111	0.034333302

these lines equal to zero, according to the Green's function values and in agreement with the fact that the plane $x = 0$ is a symmetry plane of the above defined point load problem. The computed values of u_x had a high accuracy, having been less than $4.3E(-7)$ along the first line and less than $4.6E(-6)$ along the second.

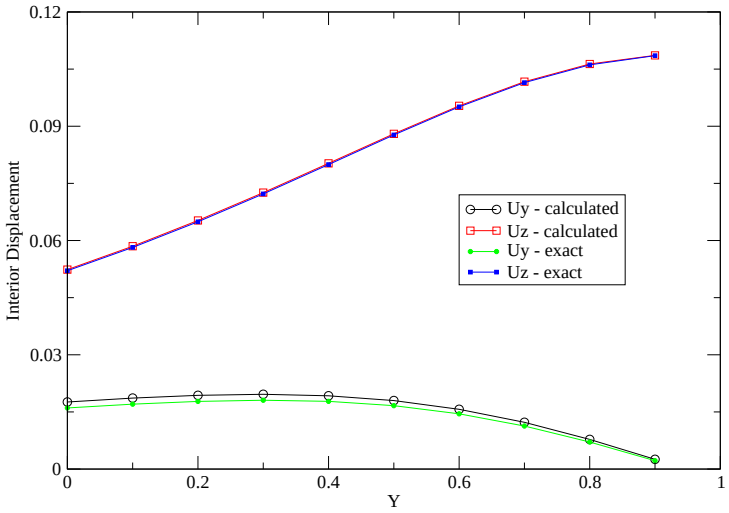

Figure 20. Interior displacement values at points $(0, y, 0)$ for $\beta = 0.2$ and point load boundary conditions.

Finally, this last calculation was repeated with $\beta = 1.0$, so that the shear modulus now varies $e^4 \doteq 54.6$ times through the sphere. The results are plotted in Figure 22 and, despite the strong variation in μ, the agreement remains excellent.

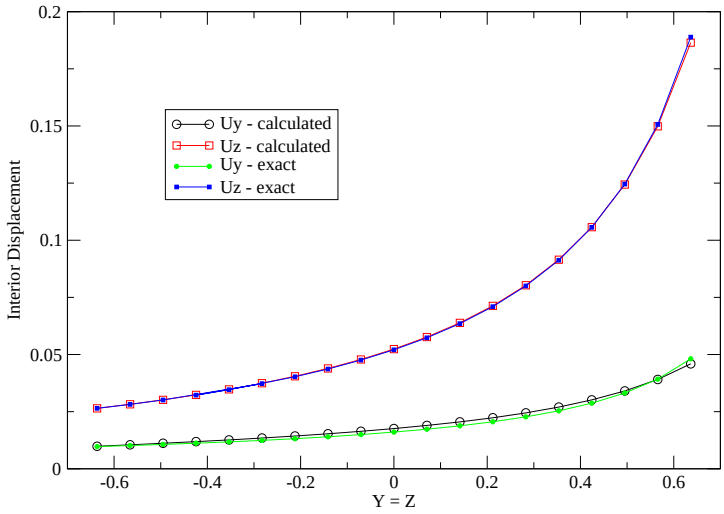

Figure 21. Interior displacement values at points $(0, y, y)$ for $\beta = 0.2$ and point load boundary conditions.

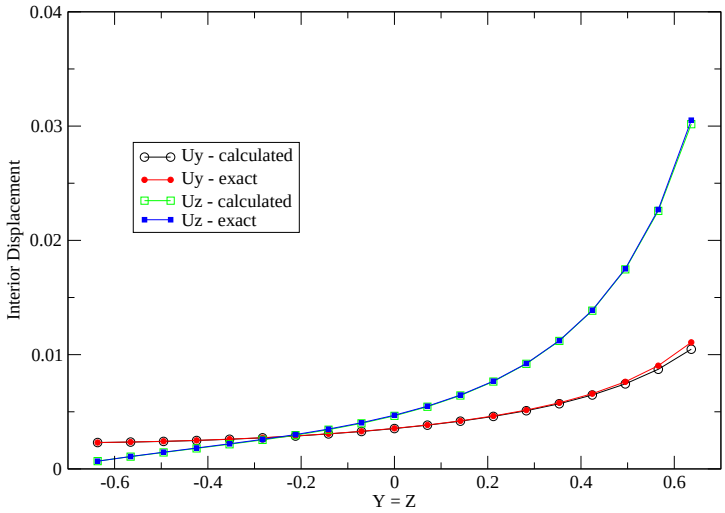

Figure 22. Interior displacement values at points $(0, y, y)$ for $\beta = 1.0$ and point load boundary conditions.

9. CONCLUSIONS

The numerical tests in this paper have established that, with one alteration, the Green's function derived in [24] is correct. Moreover, the implementation of this fundamental solution in a Galerkin boundary integral analysis is straightforward, in that the treatment of the singular integrals can be based upon existing techniques [29]. The analytical integrations can be limited to just the Kelvin solution component of the Green's function, and thus there is little difference

between this part of the analysis and that for homogeneous isotropic elasticity.

Due to inherent problems with an indirect method applied to solids with non-smooth boundaries, efficient and general boundary integral modeling of FGMs will require a direct boundary integral formulation involving the $\boldsymbol{\mathcal{T}}$ kernel (a possible exception: a better alternative to the indirect formulation, but similar in that it only relies on the Green's function, would be to use the Method of Fundamental Solutions [35]). Preliminary work has shown that the computation and implementation of the $\boldsymbol{\mathcal{T}}(Q,P)$ kernel function proceeds along the same lines as discussed herein, and this work will be reported elsewhere.

The key remaining problem for FGM analysis via boundary integral equations is computation time: at present, it is not practical, as the evaluation of the Green's function is simply too time consuming. A detailed study of the individual integrals comprising the grading term would hopefully lead to reductions in computational cost, and also possibly indicate which integrals are the most expensive. For these contributions, or maybe in fact entire grading term, it should be possible to employ the scheme proposed by Wilson and Cruse for the anisotropic Green's function [36], namely storing pre-computed values in a table and then interpolating from this table. Another possible option would be to employ a fast method, *e.g.*, fast multipole [37, 38] or fast spectral [39, 40], which requires many fewer Green's function evaluations; combining these two techniques might be very effective. It is therefore expected that, with further work, the computational cost of working with the FGM Green's function can be reduced to a reasonable level. Now that it is known that 'brute force' evaluation is successful, this work can begin.

ACKNOWLEDGMENT

The authors would like to thank P. A. Martin for very useful discussions, and for providing equation (39). This work was supported by the Spanish Ministry of Education, Culture and Sport through the projects SAB 2003-0088 (LJG), and the Spanish Ministry of Science and Technology through project MAT 2003-03315 (VM and FP). RC and LJG were also supported by the Applied Mathematical Sciences Research Program of the Office of Mathematical, Information, and Computational Sciences, U.S. Department of Energy, under contract DE-AC05-00OR22725 with UT-Battelle, LLC.

The submitted manuscript has been authored by a contractor of the U. S. Government under contract DE-AC05-00OR22725. Accordingly the U. S. Government retains a non-exclusive, royalty free license to publish or reproduce the published form of this contribution, or allow others to do so, for U. S. Government purposes.

REFERENCES

1. Miyamoto Y, Kaysser WA, Rabin BH, Kawasaki A, Ford RG. *Functionally Graded Materials: Design, Processing and Applications*, Kluwer Academic Publishers: Dordrecht, 1999.
2. Suresh S, Mortensen A. *Fundamentals of Functionally Graded Materials*, The Institute of Materials, IOM Communications: London, 1998.
3. Watari F, Yokoyama A, Saso F, Uo M, Kawasaki T. Fabrication and properties of functionally graded dental implant. *Composites Part B* 1997; **28B**:5–11.

4. Watari F, Yokoyama A, Saso F, Uo M, Ohkawa S, Kawasaki T. Elemental mapping of functionally graded dental implant in biocompatibility test. In *Proc. 4th Int. Symp. on Functionally Graded Materials*, 1997; 749–754.
5. Silva ECN, Walters MC, Paulino GH. Modeling bamboo as a functionally graded material: lessons for the analysis of affordable materials. *Journal of Materials Science* 2006; in press.
6. Vrettos C. In-plane vibrations of soil deposits with variable shear modulus: I. surface waves. *International Journal for Numerical and Analytical Methods in Geomechanics* 1990; **14**:209–222.
7. Vrettos C. Time-harmonic Boussinesq problem for a continuously non-homogeneous soil. *Earthquake Engineering and Structural Dynamics* 1991; **20**:961–977.
8. Kim JH, Paulino GH. Finite element evaluation of mixed-mode stress intensity factors in functionally graded materials. *International Journal for Numerical Methods in Engineering* 2002; **53**:1903–1935.
9. Kim JH, Paulino GH. Mixed-mode fracture of orthotropic functionally graded materials using the finite element method. *Engineering Fracture Mechanics* 2002; **69**:1769–1790.
10. Naghdabadi R, Kordkheili SAH. A finite element formulation for analysis of functionally graded plates and shells. *Archive of Applied Mechanics* 2005; **74**:375–386.
11. Anlas G, Santare MH, Lambros J. Numerical calculation of stress intensity factors in functionally graded materials. *International Journal of Fracture* 2000; **104**:131–143.
12. Santare MH, Lambros J. Use of graded finite elements to model the behavior of nonhomogeneous materials. *Journal of Applied Mechanics* 2000; **67**:819–822.
13. París F, Cañas J. *Boundary Element Method: Fundamentals and Applications*. Oxford University Press: Oxford, 1997.
14. Bonnet M. *Boundary Integral Equation Methods for Solids and Fluids*. Wiley: England, 1999.
15. Aliabadi MH. *The Boundary Element Method. Vol. II*. Wiley: Chichester, 2002.
16. Bonnet M, Guiggiani M. Comments about the paper entitled 'A generalized boundary integral equation for isotropic heat conduction with spatially varying thermal conductivity' by A. J. Kassab and E. Divo. *Engineering Analysis with Boundary Elements* 1998; **22**:235–240.
17. Divo E, Kassab AJ. Generalized boundary integral equation for heat conduction in non-homogeneous media: recent developments on the sifting property. *Engineering Analysis with Boundary Elements* 1998; **22**:221–234.
18. Shaw RP, Makris N. Green's functions for Helmholtz and Laplace equations in heterogeneous media. *Engineering Analysis with Boundary Elements* 1992; **10**:179–183.
19. Shaw RP, Manolis GD. A generalized Helmholtz equation fundamental solution using a conformal mapping and dependent variable transformation. *Engineering Analysis with Boundary Elements* 2000; **24**:177–188.
20. Berger JR, Martin PA, Mantič V, Gray LJ. Fundamental solutions for steady-state heat transfer in an exponentially graded anisotropic material. *ZAMP* 2005; **56**:293–303.
21. Gray LJ, Kaplan T, Richardson JD, Paulino GH. Green's functions and boundary integral analysis for exponentially graded materials: heat conduction. *Journal of Applied Mechanics* 2003; **70**:543-549.
22. Martin PA. On functionally graded balls and cones. *Journal of Engineering Mathematics* 2002; **42**:133–142.
23. Ang WT, Kusuma J, Clements DL. A boundary element method for a second order elliptic partial differential equation with variable coefficients. *Engineering Analysis with Boundary Elements* 1996; **18**:311–316.
24. Martin PA, Richardson JD, Gray LJ, Berger JR. On Green's function for a three-dimensional exponentially graded elastic solid. *Proceedings of the Royal Society A* 2002; **458**:1931–1947.
25. Chan YS, Gray LJ, Kaplan T, Paulino GH. Green's function for a two-dimensional exponentially graded elastic medium. *Proceedings of the Royal Society A* 2004; **460**:1689–1706.
26. Sirtori S, Maier G, Novati G, Miccoli S. A Galerkin symmetric boundary-element method in elasticity: formulation and implementation. *International Journal for Numerical Methods in Engineering* 1992; **35**:255-282.
27. Jaswon MA, Symm GT. *Integral Equation Methods in Potential Theory and Elastostatics*. Academic Press: New York, 1977.
28. Phan-Thien N, Tullock D. Completed double layer boundary element method in elasticity. *Journal of the Mechanics and Physics of Solids* 1993; **41**:1067–1086.
29. Gray LJ, Glaeser J, Kaplan T. Direct evaluation of hypersingular Galerkin surface integrals. *SIAM Journal on Scientific Computing* 2004; **25**:1534–1556.
30. Gray LJ, Salvadori A, Phan AV, Mantič V. Direct evaluation of hypersingular Galerkin surface integrals II. *Electronic Journal of Boundary Elements* 2006; **4**:105–130.
31. Sutradhar A, Paulino GH, Gray LJ. On hypersingular surface integrals in the symmetric Galerkin boundary element method: Application to heat conduction in exponentially graded materials. *International Journal for Numerical Methods in Engineering* 2005; **62**:122–157.
32. Love AEH. *A Treatise on the Mathematical Theory of Elasticity*. Dover Publications: New York, 1944.

33. Shames IH, Cozzarelli FA. *Elastic and Inelastic Stress Analysis*. Prentice Hall: Englewood Cliffs, 1992.
34. Sokolnikoff IS. *Mathematical Theory of Elasticity*. McGraw-Hill: New York, 1956.
35. Fairweather G, Karageorghis A. The method of fundamental solutions for elliptic boundary value problems. *Advances in Computational Mathematics* 1998; **9**:69–95.
36. Wilson RB, Cruse TA. Efficient implementation of anisotropic three dimensional boundary-integral equation stress analysis. *International Journal for Numerical Methods in Engineering* 1978; **12**:1383–1397.
37. Roklin V. Rapid solution of integral equation of classical potential theory. *Journal of Computational Physics* 1985; **60**:187–207.
38. Greengard L, Rokhlin V. A fast algorithm for particle simulations. *Journal of Computational Physics* 1987; **73**:325–348.
39. Pierce AP, Napier JAL. A spectral multipole method for efficient solution of large-scale boundary element models in elastostatics. *International Journal for Numerical Methods in Engineering* 1995; **38**:4009–4034.
40. Phillips JR, White JK. A precorrected-FFT method for electrostatic analysis of complicated 3-D structures. *IEEE Trans. Comput. Aided Design of Integrated Circuits and Systems* 1997; **16**:1059–1071.